Generalization of first-principles thermodynamic model: Application to hexagonal close-packed -Fe3N

Bakkedal, Morten Bjørn; Shang, Shu- Li; Liu, Zi-Kui; Somers, Marcel A. J.

Published in:
Computational Materials Science

Link to article, DOI:
10.1016/j.commatsci.2016.01.022

Publication date:
2016

Document Version
Peer reviewed version

Generalization of first-principles thermodynamic model: Application to hexagonal close-packed ε-Fe_3N

Morten B. Bakkedal[a,*], Shun-Li Shang[b], Zi-Kui Liu[b], Marcel A. J. Somers[a]

[a] *Department of Mechanical Engineering, Technical University of Denmark, Lyngby, Denmark*
[b] *Department of Materials Science and Engineering, Pennsylvania State University, University Park, PA 16802, USA*

Abstract

A complete first-principles thermodynamic model was developed and applied to hexagonal close-packed structure ε-Fe_3N. The electronic structure was calculated using density functional theory and the quasiharmornic phonon approximation to determine macroscopic thermodynamic properties at finite temperatures was generalized in terms of the partition function for any lattice of interest. Specially, thermal expansion of the hexagonal close-packed ε phase with two independent lattice parameters was studied by means of the present model and first-principles phonon calculations. The present predictions of thermal expansion of ε-Fe_3N are in good agreement with experimental data.

Keywords: First-principles, Thermodynamics, Equation of state, Quasi-harmonic phonon, Fe_3N

1. Introduction

Thermodynamics of Fe-N phases is of crucial importance in understanding material behavior observed in the practice of nitriding of iron and steels, i.e., a thermochemical surface engineering process applied to enhance wear and corrosion performance of steels. One phase of major importance is the iron-based nitride ε-Fe_2N_{1-z} developing on steel surfaces during nitriding. ε-Fe_2N_{1-z} can

*Corresponding author
Email address: mbjba@mek.dtu.dk (Morten B. Bakkedal)

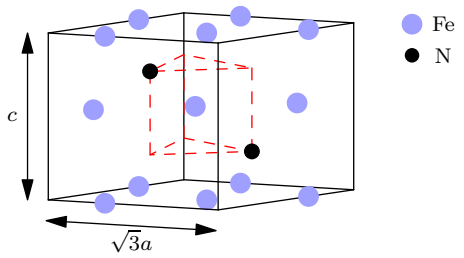

Figure 1: The hexagonal unit cell with the iron host lattice and six interstitial sites highlighted. The dashed lines connect the interstitial sites of the hexagonal unit cell of which two are occupied by nitrogen atoms. The lattice parameter a defines the distance between iron atoms in the horizontal close-packed planes.

be conceived as a hexagonal close-packed sublattice of iron atoms, where the nitrogen atoms reside in an ordered way on a sublattice formed by the octahedral interstices [1].

Fe_2N_{1-z} has been studied experimentally [2, 3, 4, 5, 6] and thermodynamic models accounting for long-range order of the nitrogen atoms were developed and fitted to experimental data [1, 7, 8]. The ground state stability at 0 K was also investigated from first-principles calculations using density functional theory [9, 10]. However, currently no first-principles thermodynamic model of the Fe_2N_{1-z} structure incorporating vibrational degrees of freedom is available in the literature. Previously, it has been discussed whether ε-Fe_2N_{1-z} for the composition range of interest, i.e., $0 \leq z \leq \frac{1}{3}$, is an equilibrium of distinct Fe_3N and Fe_2N phases. In this respect, a proper thermodynamic model of Fe_2N_{1-z} is of interest as a building block in developing a complete model for the Fe-N system from first-principles.

The occupations of interstitial sites of the Fe_3N structure by nitrogen atoms are given in Fig. 1; the space group is $P6_322$ (No. 182) and Wyckoff positions are listed in Table 1. This is the ground state configuration as determined experimentally [8] and confirmed from earlier first-principles calculations [9].

First-principles phonon calculations adopting the quasiharmonic approach provide a practical pathway to predict the thermodynamic properties [11]; in this

Table 1: Wyckoff positions of atoms in the iron sublattice (6g) and occupied interstitial sites (2c). The space group is $P6_322$ (No. 182).

6g	$(x,0,0)$, $(0,x,0)$, $(-x,-x,0)$, $(-x,0,\frac{1}{2})$, $(0,-x,\frac{1}{2})$, $(x,x,\frac{1}{2})$; $x = 0.3262$[1]
2c	$(\frac{1}{3},\frac{2}{3},\frac{1}{4})$, $(\frac{2}{3},\frac{1}{3},\frac{3}{4})$

[a] Calculation from [9].

approach vibrational states are determined by the second-order perturbation of ions. However, the direct determination of thermal expansion of a structure with two lattice parameters is challenging.

In the present work, a generalized approach based on the quasiharmonic approximation was developed and used to determine the thermal expansion of the lattice parameters of the hexagonal close-packed ε phase with atomic numbers and atomic crystal structure as the only input parameters. Here, the phonon dispersion relation was assumed to be a function of the two lattice parameters, rather than the unit cell volume, and was calculated for a range of lattice parameters to determine equilibrium properties. Numerical prerequisites were developed by providing a tractable two-dimensional equation of state for the hexagonal system, in terms of an extension to one of the commonly used equations of state [12], so that the vibrational and electronic Helmholtz free energy of the system is smoothly defined as a function of lattice parameters.

The first part of this paper presents the framework of first-principles thermodynamics and the generalization of the quasiharmonic phonon approximation. The second part develops a smooth functional expression of the thermodynamic potentials to allow determining equilibrium properties. In the third part of this paper, the predicted lattice parameters and thermal expansion coefficient are given as a function of temperature and compared to experimental data [1, 3].

2. First-principles thermodynamics

The Hamiltonian of the system is decomposed as

$$\hat{H} = \hat{H}^0 + \hat{H}^{\text{el}} + \hat{H}^{\text{ph}} + \hat{H}^{\text{el-ph}}, \tag{1}$$

with static ionic repulsion $\hat{H}^0$, an electronic part $\hat{H}^{\text{el}}$, and a vibrational part $\hat{H}^{\text{ph}}$. The electron-phonon interaction $\hat{H}^{\text{el-ph}}$ is neglected throughout this work.

In some abstract basis $|\varepsilon\omega; r\rangle$, combining vibrational ω and electronic ε eigenstates, as well as elastic displacement r, the partition function Z, which is defined as the trace of the density operator $\hat{\rho} = e^{-\beta\hat{H}}$, is given by

$$Z = \operatorname{tr}\hat{\rho} = \sum_{\omega}\sum_{\varepsilon} e^{-\beta E_{\omega\varepsilon;r}}, \tag{2}$$

where $E_{\omega\varepsilon;r}$ is the energy eigenvalue of $|\varepsilon\omega; r\rangle$, $\beta = (k_B T)^{-1}$ is the reciprocal temperature, k_B is the Boltzmann constant, and T is the absolute temperature.

2.1. Thermodynamic potentials

Thermodynamic potentials defined in terms of macroscopic variables are obtained from the partition function Eq. (2). For a given elastic displacement r, the Helmholtz free energy is

$$F_r = -\beta^{-1}\log Z. \tag{3}$$

Decomposing r into lattice parameters (a, c) as shown in Fig. 1 and ionic positions r', it follows

$$F_{ac} = \min_{r'} F_{r=(a,c,r')}, \tag{4}$$

with ions at equilibrium positions. Then, taking V_{ac} as the volume of the unit cell,

$$F(T, V) = \min_{V_{ac}=V} F_{ac} \tag{5}$$

is the Helmholtz free energy, which depends on temperature and volume.

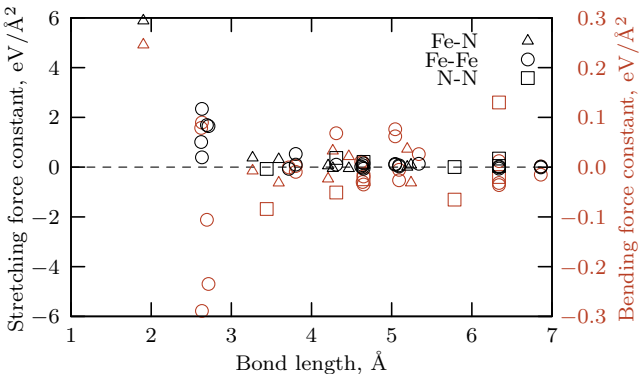

Figure 2: Calculated force constants as a function of bond length. Stretching force constants (black) and the weaker bending force constants (brown, secondary axis) for the Fe-N, Fe-Fe, and N-N bonds. Calculated for equilibrium lattice parameters. Notice that stretching one particular bond can implicitly bend another bond; hence some stretching force constants are calculated negative and some bending force constants are calculated positive.

2.2. Vibrational contribution

Phonons are quantized collective oscillations of the ions in the crystal described by

$$\hat{H}^{\mathrm{ph}} = \sum_{\mathbf{q}\lambda} \hbar\omega_{\mathbf{q}\lambda}\left(\hat{b}^{\dagger}_{\mathbf{q}\lambda}\hat{b}_{\mathbf{q}\lambda} + \frac{1}{2}\right), \tag{6}$$

where $\mathbf{q}$ is the wave vector, λ is the branch index, $\hat{b}^{\dagger}_{\mathbf{q}\lambda}$ is the phonon creation operator, and $\hat{b}_{\mathbf{q}\lambda}$ is its adjoint annihilation operator. The dispersion relation $\varepsilon_{\mathbf{q}\lambda} = \hbar\omega_{\mathbf{q}\lambda}$ depends implicitly on the elastic displacement r to allow quasiharmonic oscillations, i.e., $\omega_{\mathbf{q}\lambda}$ is determined independently for each pair of lattice parameters (a, c). Introducing this dependence is crucial in the generalization of the quasiharmonic phonon model.

The free energy is expressed in terms of the density of states $d(\omega) = \sum_{\mathbf{q}\lambda} \delta(\omega - \omega_{\mathbf{q}\lambda})$,

$$F^{\mathrm{ph}} = \int d\omega\, d(\omega)\left[\beta^{-1}\log\left(1 - e^{-\beta\hbar\omega}\right) + \frac{1}{2}\hbar\omega\right]. \tag{7}$$

The force constant matrix is determined for each pair of lattice parameters (a, c) as the Hessian of the elastic energy $E(r') = E_{0;r=(a,c,r')}$ in the remaining

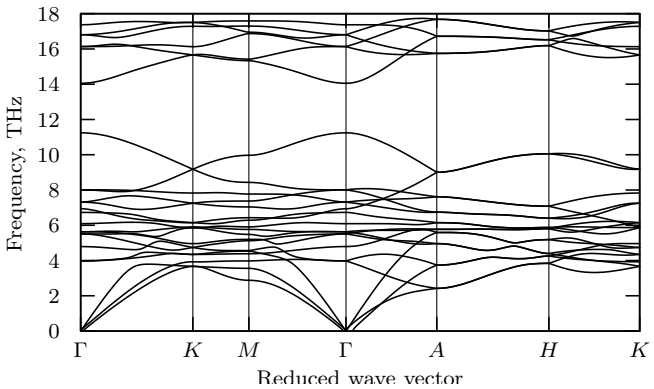

Figure 3: Phonon dispersion curve calculated for equilibrium lattice parameters.

elastic variables r', i.e., the ionic positions,

$$\Phi(jj', nn') = \frac{\partial^2 E}{\partial \mathbf{u}_{jn} \partial \mathbf{u}_{j'n'}}, \tag{8}$$

defined for pairs of ions jn and $j'n'$, where $\mathbf{u}_{jn}$ is the position of the ion j in unit cell n.

The density of states $d(\omega)$, and hence the vibrational free energy, is obtained from the force constants through the dynamic matrix [13].

2.3. Electronic contribution

The electronic free energy is determined through the spin-polarized electronic density of states $d_\sigma(\varepsilon)$ [11],

$$F^{\mathrm{el}} = -\beta^{-1} \sum_\sigma \int d\varepsilon \, d_\sigma(\varepsilon) \log\left(1 + e^{-\beta(\varepsilon - \mu)}\right), \tag{9}$$

where μ is the electronic chemical potential required to maintain charge neutrality.

3. Energy–volume equation of state

Helmholtz free energy Eq. (5) at some fixed temperature T,

$$E(V) = F(T, V), \tag{10}$$

can be determined from first-principles for any given unit cell volume V, thereby, in principle, defining a smooth function. It is infeasible to calculate this for more than a small number of points; therefore, a smooth energy–volume relationship is established by one of the many equations of state (EOS) presented in the literature [11]. In the present work, the Birch–Murnaghan equation (BM) [12],

$$E(V) = E_0 + \sum_{i=2}^{m-1} E_i \left[\left(\frac{V}{V_0} \right)^{-2/3} - 1 \right]^i, \tag{11}$$

is chosen with parameters $E_0, V_0, E_2, \ldots, E_{m-1}$, and defined so that E_0 and V_0 are the equilibrium energy and volume, respectively, and the other parameters are higher-order non-equilibrium corrections.

Since the expansion Eq. (11) can be performed for any temperature T, and since the vibrational and electronic contributions, Eq. (7) and Eq. (9), respectively, are both smoothly defined in temperature, we can assume a smoothly defined function $(T, V) \mapsto E(V)_{|T}$ in both temperature and volume.

3.1. Extension to hexagonal systems

A full description of thermodynamic equilibrium properties of the system necessitates a two-dimensional hexagonal extension of the equation of state, ideally containing the original volume-only equation in its formulation as a special case, making V and the ratio of lattice parameters $r = c/a$ natural independent variables,

$$E(V, r) = F_{ac}, \tag{12}$$

determined uniquely by Eq. (4) from the inverse of the mapping $(a, c) \mapsto (V_{ac}, c/a)$.

Having established such a relation, the lowest energy value of (V, r), or equivalently the corresponding lattice parameters (a, c), may be calculated as these change with vibrational excitations as a function of temperature.

The energy is expanded in the following steps. Firstly, the equilibrium value of $r_0(V) = \arg\min_r E(V, r)$ is expanded as

$$r_0(V) = \sum_{i=0}^{m_r-1} \rho_i \left[\left(\frac{V}{V_0} \right)^{-2/3} - 1 \right]^i, \tag{13}$$

Table 2: Equilibrium lattice parameters (a_0, c_0), equilibrium bulk modulus B_0, bulk modulus pressure derivative B_0', and volumetric thermal expansion coefficient α as a function of temperature T. Equation of state parameters are given in Table 3.

T, K	a_0, Å	c_0, Å	B_0, GPa	B_0'	α, $10^{-5}\,\mathrm{K}^{-1}$
295	2.6957	4.3379	197.2	5.5	2.85
	2.7100[b]	4.3748[b]	172.4[d]	5.7[d]	2.92[c]
300	2.6958	4.3383	197.0	5.5	2.86
	2.7108[a]	4.3783[a]			
468	2.6990	4.3508	189.2	6.1	3.31
	2.7132[b]	4.3892[b]			3.47[c]
508	2.6997	4.3543	187.1	6.3	3.40
	2.7137[b]	4.3937[b]			3.60[c]
546	2.7004	4.3577	185.0	6.5	3.48
	2.7143[b]	4.3985[b]			3.72[c]
588	2.7011	4.3618	182.6	6.6	3.57
	2.7148[b]	4.4035[b]			3.85[c]
618	2.7017	4.3649	180.9	6.8	3.64
	2.7162[b]	4.4065[b]			3.95[c]

[a] Experimental data from [1].

[b] Experimental data from [3].

[c] As determined from fit to experimental data from [3].

[d] Experimental data from [5] (ambient temperature assumed).

with parameters $\rho_0, \ldots, \rho_{m_r-1}$. Secondly, a correction to $E_0(V)$ from Eq. (11) is introduced to second order in r, noting that $\frac{\partial E}{\partial r}(V, r_0(V))$ vanishes,

$$E(V,r) = E_0(V)\left[1 + \frac{1}{2}\gamma(V)\big(r - r_0(V)\big)^2\right]. \tag{14}$$

The curvature itself is expanded as

$$\gamma(V) = \sum_{i=0}^{m_c-1} \gamma_i \left[\left(\frac{V}{V_0}\right)^{-2/3} - 1\right]^i, \tag{15}$$

with parameters $\gamma_0, \ldots, \gamma_{m_c-1}$.

The minimum energy curve $V \mapsto (V, r_0(V))$ is easily calculated, and by Eq. (14) equals the original volume-only equation of state, so that derived thermodynamic properties such as pressure p, bulk modulus B, and its derivative B' can be calculated directly from Eq. (11) [11]. The thermal expansion coefficient can also be calculated by introducing temperature dependence as explained above.

However, the tractability of the proposed extended equation of state makes the fitting procedures somewhat more complicated, and non-linear optimization is required; details are given in Sec. 4.

4. Computational details

First-principles calculations were performed using density functional theory (DFT) as implemented in the Vienna Ab initio Simulation Package (VASP) [14, 15]. The electron-ion interactions were described by the full potential frozen-core PAW method [16, 17], and the exchange-correlation was treated within the GGA of Perdew–Burke–Ernzerhof (PBE) [18]. Monkhorst–Pack sampling [19] of basis set wave vectors in the Brillouin zone was performed with $11 \times 11 \times 11$ mesh k-points centered on the Γ point to avoid breaking the hexagonal symmetry. Methfessel–Paxton of first order was used with smearing width 0.2 eV [20]. The plane wave basis set was truncated at 520 eV and the energy convergence criterion for electronic self-consistency was 10^{-5} eV per atom.

First-principles energies were obtained in two steps. Firstly, ionic positions relative to the fixed unit cell were relaxed in 45 relaxation steps using the conjugate-gradient algorithm [21]. Secondly, accurate energies were calculated with the Vosko–Wilk–Nusair interpolation of the correlation part of the exchange correlation functional [22]. First-principles energies were calculated for 130 distinct pairs lattice parameters spanning a fine mesh around minimum energy values (cf. Fig. 4).

Phonon calculations were carried out by the supercell method [23] in a unit cell of 48 iron host atoms obtained by repeating the original unit cell $2 \times 2 \times 2$ times. Force constants were calculated with exact second-order energy derivatives using density functional perturbation theory (DFPT) [24], also as implemented in VASP. A Γ centered mesh of $4 \times 4 \times 4$ k-points was used. To obtain accurate force constants, the energy convergence criterion for electronic self-consistency was lowered to 10^{-8} eV per atom. A slightly lower plane wave basis set truncation at 500 eV was used for the phonon calculation to make the memory requirements of larger supercell problem manageable. Accurate relaxation of ionic positions relative to the supercell were performed before force constants were obtained by DFPT. As calculation of force constants is significantly more expensive computationally, this was only performed for 62 distinct pairs of lattice parameters, excluding points far away from equilibrium and chosen in anticipation of preference for larger lattice parameters for higher temperatures.

The phonon density of states integration was performed with Yphon [25]. Ipopt [26] and the author's FuncLib library was used for non-linear optimization.

5. Results and discussion

5.1. Force constants and vibrational contributions

Second-order changes in energy corresponding to perturbation of one pair of ionic positions were determined by Eq. (8), as calculated by the supercell linear response method. By choosing a basis with one basis vector in the direction of the separation, diagonal entries in the matrix of force constants correspond to

stretching and bending, respectively. Independent force constant matrices were determined for each pair of lattice parameters in the quasiharmonic phonon approximation.

Fig. 2 shows the calculated force constants for the equilibrium lattice parameters; similar results for other pairs of lattice parameters were obtained. Perturbing an ion in stretching direction of one bond may result in a perturbation of the same ion in one of the bending directions of another bond, and vice versa. This explains the positive bending Fe-N force constant and negative N-N stretching force constant despite each ions are at equilibrium positions where first-order derivatives vanishes. In this case, the stretching directing of the Fe-N bond is almost in the plane of the bending directions of the N-N bond.

The phonon density of states $d(\omega)$ was obtained from the force constants as described in Sec. 2.2. This allows the vibrational contribution to the Helmholtz free energy to be calculated by Eq. (7). The phonon dispersion relation along important symmetry of the hexagonal unit cell directions is given in Fig. 3 for the equilibrium lattice parameters. Similar dispersion relation curves were obtained for other pairs of lattice parameters.

5.2. Fitting the equation of state

A five-parameter Birch–Murnaghan equation of state was chosen, augmented with three additional parameters ($m_r = 2, m_c = 1$) to fit the entire energy–lattice parameter surface. Parameters were obtained by minimizing the squared deviations,

$$\eta = \sqrt{\sum_{i=1}^{k} \frac{\left(E^{\mathrm{fit}}(V_i, r_i) - E(V_i, r_i)\right)^2}{k}}, \tag{16}$$

of Helmholtz free energies at (V_i, r_i). The fitting was repeated for any temperature of interest, resulting in a smooth temperature dependence.

Table 2 lists predicted equilibrium lattice parameters, bulk modulus, pressure derivative of bulk modulus, and thermal expansion evaluated for selected temperatures. Comparison to experimental data available in the literature is

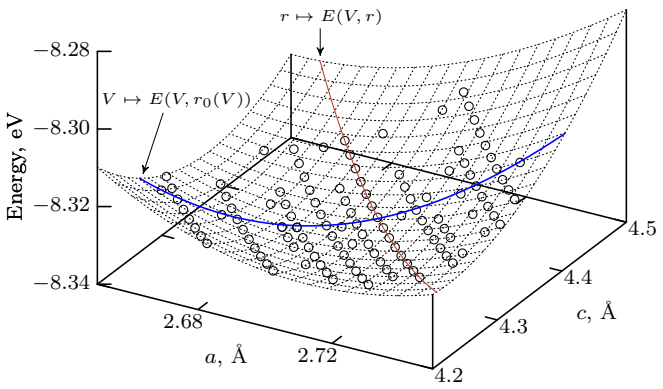

Figure 4: First-principles ground state energies per atom for various lattice parameters (a, c) (circle) and the fitted extended equation of state $(a, c) \mapsto E(V_{ac}, c/a)$ visualized as a function of lattice parameters (dotted mesh). Projection $V \mapsto E(V, r_0(V))$ through equilibrium lattice parameters as a function of imposed volume (thick blue line) and projection $r \mapsto E(V, r)$ for some fixed volume $V = 10.3\,\text{Å}^3$ (thin brown line). The quasiharmonic phonon model allows phonon free energies to be calculated for each of these points and the extended equation of state to be refitted for any $T > 0$.

Table 3: Equation of state parameters as described by Eq. (11), Eq. (13), and Eq. (15) corresponding to predicted values listed in Table 2. Notice that the first-order energy expansion term as a function of volume vanishes by construction. The ratio of lattice parameters at equilibrium volume satisfies $r_0 = c_0/a_0 = \rho_0$. The root-mean-squared fitting error per atom η of the equation of state is also given.

T, K	V_0, Å^3	E_0, eV	E_2/E_0	E_3/E_0	E_4/E_0	ρ_0	ρ_1	γ_0	η, meV
295	10.238	−8.3137	−1.7050	−1.2473	27.784	1.6092	0.0060788	−0.30256	0.0840
300	10.239	−8.3150	−1.7032	−1.2605	27.794	1.6093	0.0041618	−0.30203	0.0843
468	10.293	−8.3674	−1.6340	−1.7322	27.516	1.6120	−0.068319	−0.28293	0.109
508	10.307	−8.3824	−1.6153	−1.8487	27.313	1.6129	−0.087758	−0.27811	0.118
546	10.320	−8.3973	−1.5966	−1.9598	27.085	1.6137	−0.10699	−0.27344	0.128
588	10.335	−8.4147	−1.5752	−2.0827	26.796	1.6148	−0.12914	−0.26820	0.140
618	10.346	−8.4276	−1.5592	−2.1704	26.571	1.6156	−0.14555	−0.26440	0.148

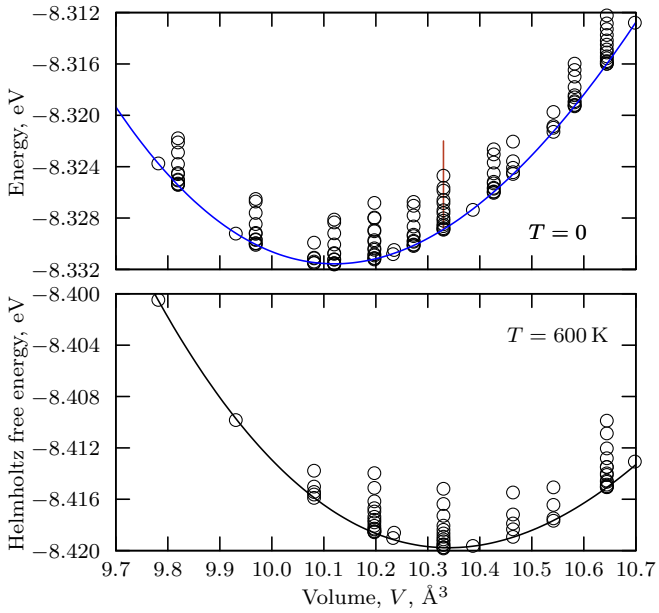

Figure 5: (Upper) First-principles energies grouped by volume per atom V, i.e., energies for multiple pairs of lattice parameters (a, c) with the same volumes V_{ac} have been calculated. The view corresponds to the surface plot of Fig. 4 seen from the side along the equilibrium curve $V \mapsto E(V, r_0(V))$ (blue line). The equilibrium curve of the fitted extended equation of state accurately fits through the lowest energy points for each V. (Lower) Same calculation repeated for the Helmholtz free energy F_{ac} including electronic and vibrational contributions at $T = 600\,\mathrm{K}$. A smaller selection of points has been calculated than for $T = 0$.

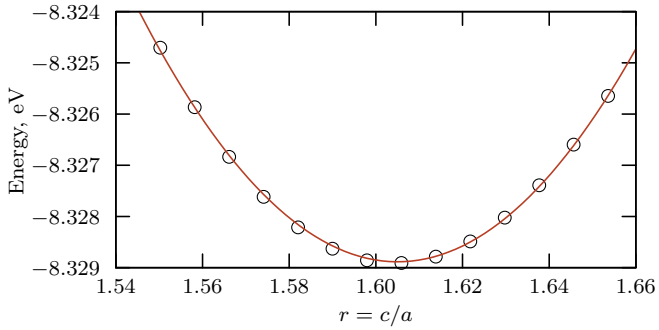

Figure 6: First-principles energies for volume $V = 10.3\,\mathrm{Å}^3$. The view corresponds to the surface plot of Fig. 4 seen along the constant-volume curve $r \mapsto E(V, r)$ (brown line). Excellent fit also in this direction. Similar fits are obtained for other values of V and for $T > 0$. Equilibrium ratio $r = c/a$ is correctly reproduced by the fitted equations of state.

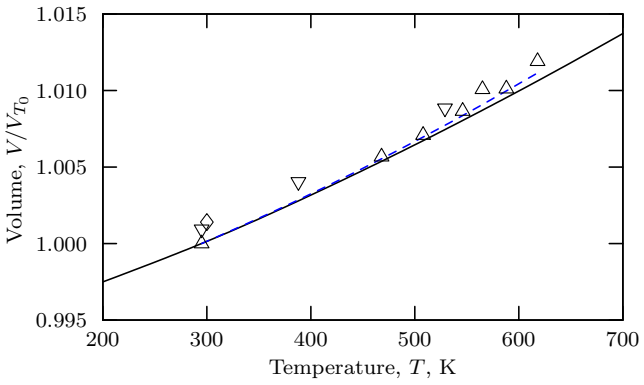

Figure 7: Predicted equilibrium volume V (solid line) as a function of temperature T. Experimental data from [3], heating (triangle up) and cooling (triangle down) phases, respectively, with Eq. (19) fitted to the values (dashed blue line), and from [1] (diamond). Normalized to volume at reference temperature $T_0 = 295\,\mathrm{K}$.

provided [1, 3, 5]. The complete set of equation of state parameters and fitting errors are given in Table 3 for reference.

Fig. 4 shows the calculated first-principles energies and energy–lattice parameter surface obtained from the fitted extended equation of states. Fig. 5 shows a projection of the calculated energy surface at the equilibrium value of $r = c/a$, $V \mapsto E(V, r_0(V))$, for given imposed unit cell volumes V. Projections are given for $T = 0$ and $T = 600\,\mathrm{K}$, clearly showing the expected thermal expansion predicted by the quasiharmonic phonon model. Fig. 6 shows a projection for fixed volume and varying values of $r = c/a$.

The fitting errors in Table 3 show that it is possible to fit the entire energy surface with three additional parameters while obtaining a small fitting error $\eta \simeq 0.1\,\mathrm{meV}$. Also, the fitting errors obtained here are almost the same as that of a pure five-parameter Birch–Murnaghan equation through points near equilibrium values $r_0(V)$ only, with very similar equilibrium curves $V \mapsto E(V, r_0(V))$.

5.3. Lattice parameters and thermal expansion

The equation of state extended to hexagonal systems, as described in Sec. 3, makes it possible to calculate equilibrium values of (V, r) or, equivalently, the

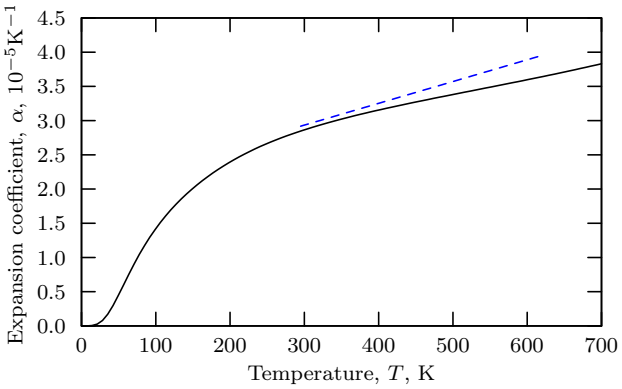

Figure 8: Predicted volumetric thermal expansion coefficient α (solid line) as a function of temperature T compared to fit to experimental data (dashed blue line); see Fig. 7 for description. The difference at high temperatures may be due to anharmonicity.

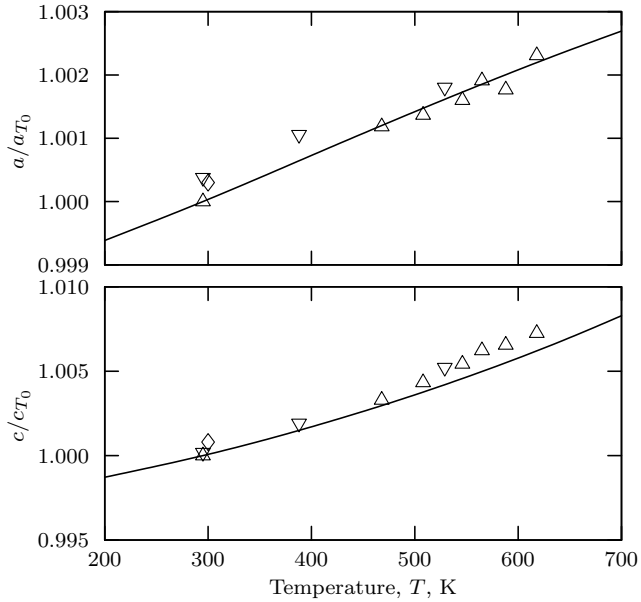

Figure 9: Predicted lattice parameters (solid line). Experimental data from [3], heating (triangle up) and cooling (triangle down) phases, respectively, and from [1] (diamond). Normalized to lattice parameters at reference temperature $T_0 = 295\,\mathrm{K}$.

corresponding lattice parameters (a, c), as a function of temperature, corresponding to the minimum of the two-variable function in Fig. 4. Equilibrium lattice parameters are listed in Table 2 for various temperatures.

The equilibrium volume function,

$$V(T) = \arg\min_{V'} F(T, V'), \tag{17}$$

is shown in Fig. 7 and compared with experimental data published in the literature [1, 3]. The volumetric thermal expansion coefficient is given by

$$\alpha(T) = \frac{1}{V(T)} \frac{dV}{dT}(T), \tag{18}$$

and the predicted expansion coefficient is given in Fig. 8 as a function of temperature. A functional form

$$V(T) = V(T_0) e^{\int_{T_0}^{T} (\alpha_0 + \alpha_1 T') dT'} \tag{19}$$

has been suggested [27] to obtain an estimate of the expansion coefficient from experimental data of lattice parameters, i.e., a polynomial expansion of $\alpha(T)$ in T. Fig. 7 and Fig. 8 show the resulting fit to experimental data and the corresponding expansion coefficient Eq. (18), respectively.

The lattice parameter pair (a, c) that minimizes Eq. (4) is given in Fig. 9. The relative deviation in the present work compared to experimental lattice parameters at ambient temperature is $(-0.53\%, -0.84\%)$. This compares to $(-0.81\%, -1.30\%)$ obtained in [9] and $(+0.50\%, -0.89\%)$ obtained in [10] with the optimal choice of the empirical parameter in the GGA+U exchange-correlation functional.

The better agreement of the present model with experimental data as compared to earlier work was obtained, because expansion of the unit cell due to vibrational excitations was accounted for. The difference between predicted equilibrium values at $T = 0$ in the present work and those in [9] is due to the quantum effect of zero-point vibrations originating from the last term in Eq. (6).

The predicted unit cell volume given in Fig. 7, the thermal expansion coefficient given in Fig. 8, and the lattice parameters given in Fig. 9, obtained

Table 4: Predicted energy per atom E, volume per atoms V, and equilibrium ratio c/a as a function of temperature T and pressure p.

T, K	p, GPa	E, eV	V, Å^3	c/a
295	0.0	−8.314	10.24	1.6092
			10.47[a]	1.6125[a]
			10.43[b]	1.6143[b]
295	4.7	−8.310	10.01	1.6093
			10.19[a]	1.6141[a]
295	10.4	−8.299	9.76	1.6094
			9.92[a]	1.6154[a]
295	15.6	−8.281	9.54	1.6095
			9.79[a]	1.6164[a]
295	18.5	−8.268	9.42	1.6095
			9.68[a]	1.6184[a]

[a] Experimental data from [5] (ambient temperature assumed).

[b] Experimental data from [3].

from the generalized quasiharmonic phonon approximation show good agreement with predicted thermal expansion compared to experimental data in the literature [1, 3].

5.4. Volume–pressure relationship

The tractability of the model also allows prediction of equilibrium properties for imposed positive pressure $p > 0$ for any given temperature. In Table 4 unit cell volume and lattice parameter ratio c/a are listed and compared to high-pressure experimental data [5]. The sample is prepared at high-temperature and quenched to ambient temperature. Other experimental data in the literature suggest configurational disordering of interstitial site occupations at elevated temperatures [4], which would be locked in the quenching process. The present model does not account for such configurational disordering. Also notice that the

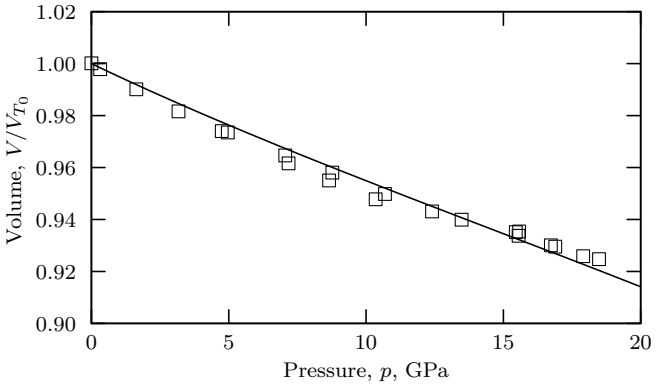

Figure 10: Predicted unit cell volume (solid line) as a function of pressure. Experimental data from [5] (square). Normalized to volume at reference temperature $T_0 = 295\,\mathrm{K}$.

volume–pressure experimental data are obtained from a sample with a slightly higher nitrogen concentration with the composition $Fe_3N_{1.05}O_{0.017}$.

Fig. 10 shows the predicted change in volume as a function of pressure in good agreement with the experimental data. The model does not predict significant change in the ratio of lattice parameter c/a as the imposed pressure is increased. Moreover, the predicted bulk modulus and its derivative with respect to pressure listed in Table 2 are in good agreement with experimental data and provide improvements compared to previous first-principles calculations [5].

6. Conclusions

A thermodynamic model was developed for the hexagonal close-packed ε-Fe_3N structure, and lattice parameters and thermal expansion coefficient were calculated using the proposed two-dimensional equation of state. The expansion coefficient predicted by the quasiharmonic phonon approximation is in good agreement with experimental data. Also predicted volume–pressure relationship is in good agreement with high-pressure experimental data.

Acknowledgments

The authors are grateful to The Danish Council for Independent Research (FTP) for financial support under grant No. 11-106293. First-principles calculations were performed at the Computing Center at the Technical University of Denmark. Thanks are owed to the Phases Research Lab group at Pennsylvania State University for productive discussions. Credit is also given to Yi Wang from Pennsylvania State University for the Yphon tool.

References

[1] M. A. J. Somers, B. J. Kooi, L. Maldzinski, E. J. Mittemeijer, A. A. van der Horst, A. M. van der Kraan, N. M. van der Pers, Thermodynamics and long-range order of interstitials in an h.c.p. lattice: Nitrogen in ε-Fe_2N_{1-z}, Acta Mater. 45 (5) (1997) 2013–2025.

[2] K. H. Jack, The iron-nitrogen system: the crystal structures of ε-phase iron nitrides, Acta Cryst. 5 (4) (1952) 404–411.

[3] A. Leineweber, H. Jacobs, F. Hüning, H. Lueken, H. Schilder, W. Kockelmann, ε-Fe_3N: magnetic structure, magnetization and temperature dependent disorder of nitrogen, J. Alloys Compd. 288 (1) (1999) 79–87.

[4] T. Liapina, A. Leineweber, E. J. Mittemeijer, W. Kockelmann, The lattice parameters of ε-iron nitrides: lattice strains due to a varying degree of nitrogen ordering, Acta Mater. 52 (1) (2004) 173–180.

[5] R. Niewa, D. Rau, A. Wosylus, K. Meier, M. Hanfland, M. Wessel, R. Dronskowski, D. A. Dzivenko, R. Riedel, U. Schwarz, High-pressure, high-temperature single-crystal growth, ab initio electronic structure calculations, and equation of state of ε-Fe_3N_{1+x}, Chem. Mater. 21 (2) (2009) 392–398.

[6] S. Kurian, N. S. Bajbhiye, S. K. Date, Investigation of different iron sites in ε-Fe_yN ($2 < y < 3$) nanoparticles using mössbauer spectroscopy, J. Phys.: Conf. Ser. 217 (2010) 012107.

[7] B. J. Kooi, M. A. J. Somers, E. J. Mittemeijer, Thermodynamics and long-range order of interstitials in a hexagonal close-packed lattice, Metall. Mater. Trans. A 25 (12) (1994) 2797–2814.

[8] M. I. Pekelharing, A. Böttger, M. A. J. Somers, M. P. Steenvoorden, A. M. van der Kraan, E. J. Mittemeijer, Modeling thermodynamics of Fe-N phases: Characterization of ε-Fe_2N_{1-z}, Materials Science Forum 318–320 (1999) 115–120.

[9] S. L. Shang, A. J. Böttger, Z. K. Liu, The influence of interstitial distribution on phase stability and properties of hexagonal ε-Fe_6C_x, ε-Fe_6N_y and ε-$Fe_6C_xN_y$ phases: A first-principles calculation, Acta Mater. 56 (4) (2008) 719–725.

[10] Y. J. Shi, Y. L. Du, G. Chen, First-principles study on the elastic and electronic properties of hexagonal ε-Fe_3N, Comp. Mater. Sci. 67 (2013) 341–345.

[11] S. L. Shang, Y. Wang, D. E. Kim, Z. K. Liu, First-principles thermodynamics from phonon and Debye model: Application to Ni and Ni_3Al, Comp. Mater. Sci. 47 (4) (2010) 1040–1048.

[12] F. D. Murnaghan, Finite deformation of an elastic solid, Amer. J. Math. 59 (1937) 235–260.

[13] M. Dove, M. Dove, Introduction to Lattice Dynamics, Cambridge University Press, 2005.

[14] G. Kresse, J. Furthmüller, Efficiency of ab-initio total energy calculations for metals and semiconductors using a plane-wave basis set, Comp. Mater. Sci. 6 (1996) 15–50.

[15] G. Kresse, J. Furthmüller, Efficient iterative schemes for ab initio total-energy calculations using a plane-wave basis set, Phys. Rev. B 54 (16) (1996) 11169–11186.

[16] P. E. Blöchl, Projector augmented-wave method, Phys. Rev. B 50 (24) (1994) 17953–17979.

[17] G. Kresse, D. Joubert, From ultrasoft pseudopotentials to the projector augmented-wave method, Phys. Rev. B 59 (3) (1999) 1758–1775.

[18] J. P. Perdew, K. Burke, M. Ernzerhof, Generalized gradient approximation made simple, Phys. Rev. Lett. 77 (18) (1996) 3865–3868.

[19] H. J. Monkhorst, J. D. Pack, Special points for Brillouin-zone integrations, Phys. Rev. B 13 (12) (1976) 5188–5192.

[20] M. Methfessel, A. T. Paxton, High-precision sampling for brillouin-zone integration in metals, Phys. Rev. B 40 (6) (1989) 3616–3621.

[21] W. H. Press, B. P. Flannery, S. A. Teukolsky, W. T. Vetterling, Numerical Recipes, Cambridge University Press, New York, 1986.

[22] S. H. Vosko, L. Wilk, M. Nusair, Accurate spin-dependent electron liquid correlation energies for local spin density calculations: a critical analysis, Can. J. Phys. 58 (8) (1980) 1200–1211.

[23] A. van de Walle, G. Ceder, The effect of lattice vibrations on substitutional alloy thermodynamics, Rev. Mod. Phys. 74 (1) (2002) 11–45.

[24] S. Baroni, S. de Gironcoli, A. Dal Corso, P. Giannozzi, Phonons and related crystal properties from density-functional perturbation theory, Rev. Mod. Phys. 73 (2) (2001) 515–562.

[25] Y. Wang, J. J. Wang, W. Y. Wang, Z. G. Mei, S. L. Shang, L. Q. Chen, Z. K. Liu, A mixed-space scheme to the direct method for phonons in polar materials, J. Phys. Cond. Mat. 22 (20) (2010) 202201.

[26] A. Wächter, L. T. Biegler, On the implementation of a primal-dual interior point filter line search algorithm for large-scale nonlinear programming, Math. Prog. 106 (1) (2006) 25–57.

[27] Y. Fei, Thermal expansion, in: T. J. Ahrens (Ed.), Mineral Physics & Crystallography: A Handbook of Physical Constants, American Geophysical Union, 2013, pp. 29–44.